Phosphodiester hydrolysis computed for cluster models of enzymatic active sites

Hossein Batebi and Petra Imhof*

October 19, 2016

Institute for Theoretical Physics

Free University Berlin

Arnimallee 14

D-14195 Berlin

Germany

Abstract

Computation of phosphodiester hydrolysis in different models with one or two metal ions, representing typical active site architectures of nucleases, reveal an associative mechanism to be favorable in all of the cases studied in this work. Direct attack of the nucleophilic water molecule with proton transfer to the phosphate group is facilitated by an extra positive charge as provided by a metal ion located at the attack site or a positively charged histidine residue whereas no such contribution can be observed on leaving group departure. A major catalytic effect is found by proton transfer from the nucleophilic water molecule to a histidine-aspartate cluster. Attack of the thus generated hydroxide ion on the phosphate group is just sufficiently stabilized by the metal ions to allow subsequent P–O bond dissociation.

Introduction

Phosphodiester hydrolysis is the fundamental reaction of endonuclease enzymes cleaving the backbone of DNA and RNA, usually at a recognition site such as a specific sequence (in e.g. restriction enzymes [1]), at an abasic site (such as the apurinic/apyrimidinic (AP) endonuclease in the Base excision repair system) [2], or escherichia coli endonuclease IV (endoIV-DNA) [3] or endonuclease III homologue 1 (NTH1) that initiates the repair by β-elimination [4]. Moreover, phoshopdiester

*To whom correspondence should be addressed

cleavage can also occur in ribozymes, i.e. catalytic RNA, acting as ribonucleases [5–7].Cleavage of the phosphodiester backbone uncatalyzed in water, enzymatic reaction or RNA-catalyzed attracted many scientists' attention during the last decade [8–30]. The two extremes of a phosphate hydrolysis reaction are through an associative mechanism in which the first step is the nucleophilic attack that results in the formation of a pentacovalent molecular geometry. The second step is then the actual cleavage of the scissile P–O bond. In contrast, the first step of the alternative, dissociative mechanism is the P–O bond scission, leaving a trigonal pyramidal metaphosphate intermediate that is processed to the product via nucleophilic attack. Several intermediate mechanisms, such as a concerted bond breaking/bond formation are, however, conceivable. Depending on the nature and position of active site residues surrounding the scissile phosphate, group nucleophile activation or leaving group departure, and thereby a more associative or more dissociative mechanism, may be favored.

Available high-resolution X-ray structures of many endonuclease enzymes in complex with target DNA or RNA or substrate analogues [31–35] and various biochemical studies have shown that metal cofactors are essential for the enzymatic phosphodiester cleavage [36–39]. The metal ions not only play a direct role in the chemical step but also influence the binding interaction of the enzyme with the DNA or RNA [40,41]. For some endonucleases different structures with different numbers of metal ions have been solved by X-ray crystallography under varying conditions [42–47]. The exact number of metal ions required for catalysis and their exact role are, however, are still not clear [48, 49].

In order to elucidate the putative role Magnesium cofactors and other residues which are typically found in active sites of endonuclease enzymes play in the cleavage of a phosphate backbone, we have performed quantum mechanical calculations of reaction pathways based on different cluster models mimicking such active sites of endonuclease enzymes (see Fig. 1). These rather small models can mimic an enzymatic active site in a protein only to a limited extend. For instance, the heterogeneous electrostatic environment of protein residues farther from the active site is neglected, and the protein's flexibility cannot be taken into account. We follow here a "reductionist approach" in which the most frequent components of endonuclease active sites are gathered and possible mechanisms are evaluated. The goal is to elucidate the catalytic effect of the building blocks, metal ions and amino acid residues, in a minimalistic (cluster) model that can be regarded as a universal, but necessarily simplistic, endonuclease. The cluster models include either one or two metal ions and also vary in the number and position of amino acid residues, the number of water molecules involved in the metal ion coordination, and in the protonation state of a catalytically important histidine residue. Histidine residues may catalyze the reaction via activating

the nucleophile through deprotonation or facilitating leaving group departure through protonation as has been discussed widely in the context of phosphodiester backbone cleavage [50–52] and it is therefore plausible to consider the impact of different protonation states of histidine in the reaction pathways. Aspartate and glutamate are common amino acid residues in active sites of nucleases that are important in positioning the metal cofactors but may also act as general base/general acid1.

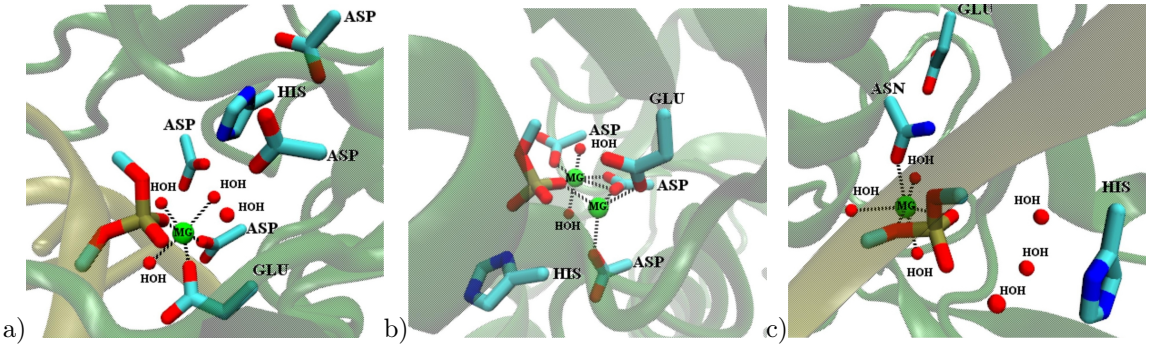

Figure 1: Active-site residues in nuclease enzymes a) human APE1 endonuclease-DNA substrate complex with one magnesium ion b) nuclease domain of 3'hExo, bound to rAMP with two magnesium ions c) intron-encoded homing endonuclease I-PPOI (H98A)/DNA homing site complex with one magnesium ion. Only the side chains of the active site amino acids and the phosphate group are shown in licorice representations. The metal ions and water molecules are depicted as green or red spheres, respectively. The protein environment and the nucleic acids are indicated by a cartoon representation.

In this paper we report calculations of phosphate hydrolysis mechanisms in cluster models of different size and composition. We find associative mechanisms to be favorable in which the direct attack of the nucleophilic water molecule with proton transfer to the phosphate group is facilitated by a second metal ion or a positively charged histidine residue whereas no catalytic effect on leaving group departure is observed. The energetically most favorable mechanism is initiated by proton transfer from the nucleophilic water molecule to a histidine-aspartate cluster. The nucleophilic attack is stabilized by the metal ions in such a way that formation of a pentacovalent intermediate is feasible while still allowing subsequent P–O bond dissociation. This balance in stabilization and weakening of P–O bonds is achieved by a delicate structural arrangement of metal ions and active site residues.

Methods

We have set up cluster models with one and two magnesium ions and variations of amino acid residues.For the one-metal models, a first type includes a protonated histidine side chain (1Mg-Hsp), and a second type contains a neutral histidine side chain (1Mg-Hsd) (see Fig.2). The two-

metal models, termed 2Mg, have been setup with neutral histidine (see Figure3). The single magnesium ion is coordinated by one glutamate and one aspartate residue, one oxygen atom of the phosphate group and a water molecule. Motivated by several high resolution crystal structures of the active sites of endonuclease enzymes [31–35], the magnesium ion is positioned either on the "attack site", binding to O2P, and termed MgA, or on the "departure site", coordinated by O1P and labeled as MgD (see Figure 2). The cluster models are inspired by actual enzymatic active sites, such as those shown in 1. They are, however, not based on any particular crystal structure (pdb file) but created artificially.

In the two-metal models, the glutamate residue bridges the two magnesium ions, here also called MgA and MgD for "attack-site" and "departure site", respectively. Both ions are coordinated by the same oxygen atom of the phosphate group (O1P). Further ligands are one aspartate residue, and two water molecules for each metal ion in models 2Mg-Hsd-Glu-2Asp and 2Mg-Hsd-Glu-2Asp-1Asp, respectively. In model 2Mg-Hsd-Glu-3Asp the second water ligand on MgD has been replaced by an aspartate residue and in model 2Mg-Hsd-Glu-1Asp the bidentate aspartate ligand on MgD has been replaced by two water molecules (see Figure 3).

The 1Mg-Hsd models and the 2Mg model have been setup in an additional variant, extended by one more aspartate residue. In the one-metal case, this aspartate residue has been placed in a position hydrogen-bonded to the histidine residue. In the two-metal case, the extra aspartate residue is either positioned in hydrogen-bond distance to the histidine residue (2Mg-Hsd-Glu-2Asp-1Asp), similar to the one-metal scenario, or it replaces a metal-coordinating water molecule (2MG-Hsd-Glu-3ASP).

Table 1 lists all models and mechanisms computed in this work. The nomenclature for the mechanisms is as follows: 1Mg or 2Mg for models with one or two magnesium ions, respectively, in the one-metal models 1MgA refers to a magnesium ion located at the attack site whereas 1MgD refers to a magnesium ion located at the departure site. he further labels -p, -d, -h refer to a mechanisms with protonated histidine, neutral histidine and direct nucleophilic attack, and neutral histidine-assisted nucleophilic attack, respectively. In the two-metal case, mechanisms for models with three, two, or one aspartate residues, corresponding to the labels -d3, -d2, and, -d1, respectively have been computed. The label -h again refers to a histidine-assisted mechanism (in a model with three aspartate residues). States along a mechanism are labeled reactant_XX, TS1_XX, Int2_XX, product_XX, etc, for the reactant, first transition state, second intermediate, and product state of mechanism XX, respectively.

In order to model an architecture that mimics the one in proteins, all amino acid residues were modeled keeping the positions of those C-atoms fixed that represent Cβ atoms, hence serving as

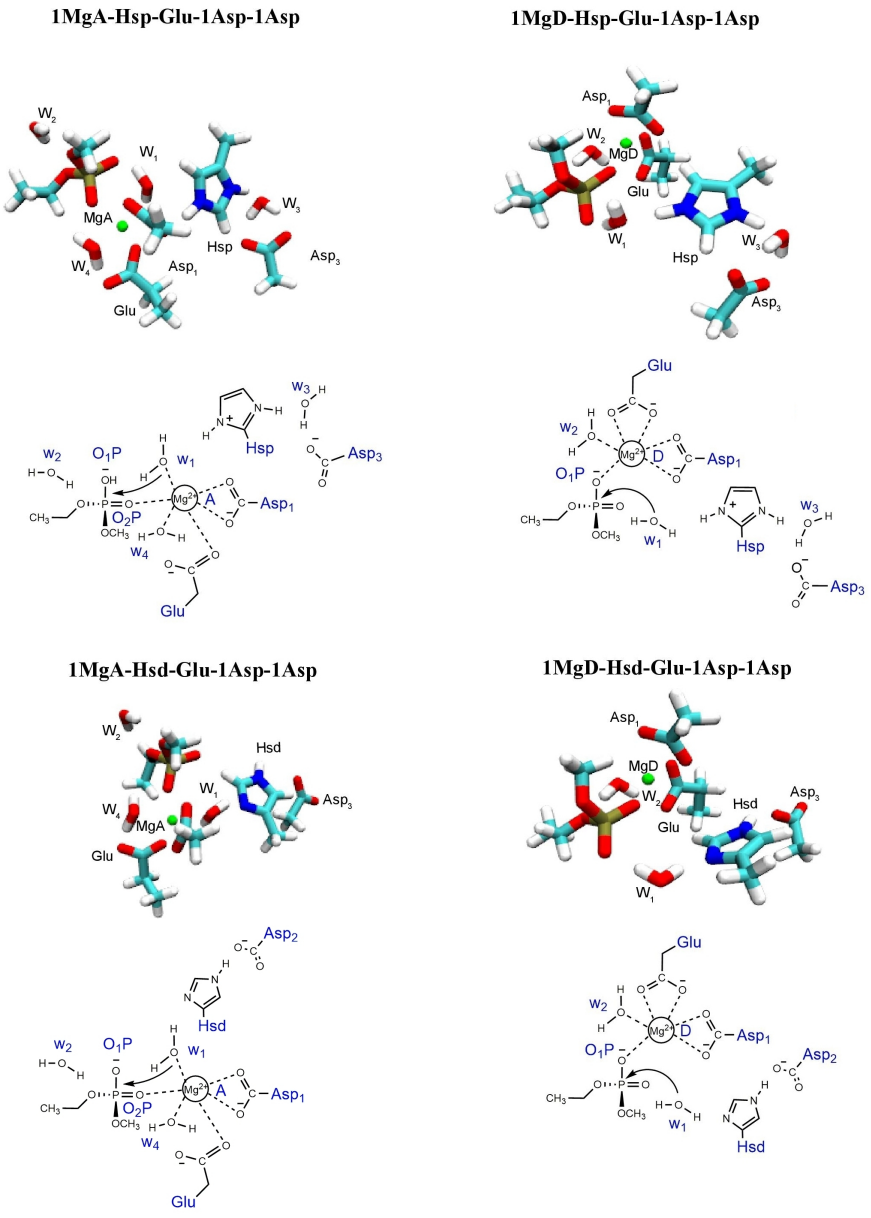

Figure 2: Reactant states for one-metal models. The scheme indicates the attack by the nucleophilic water molecule.

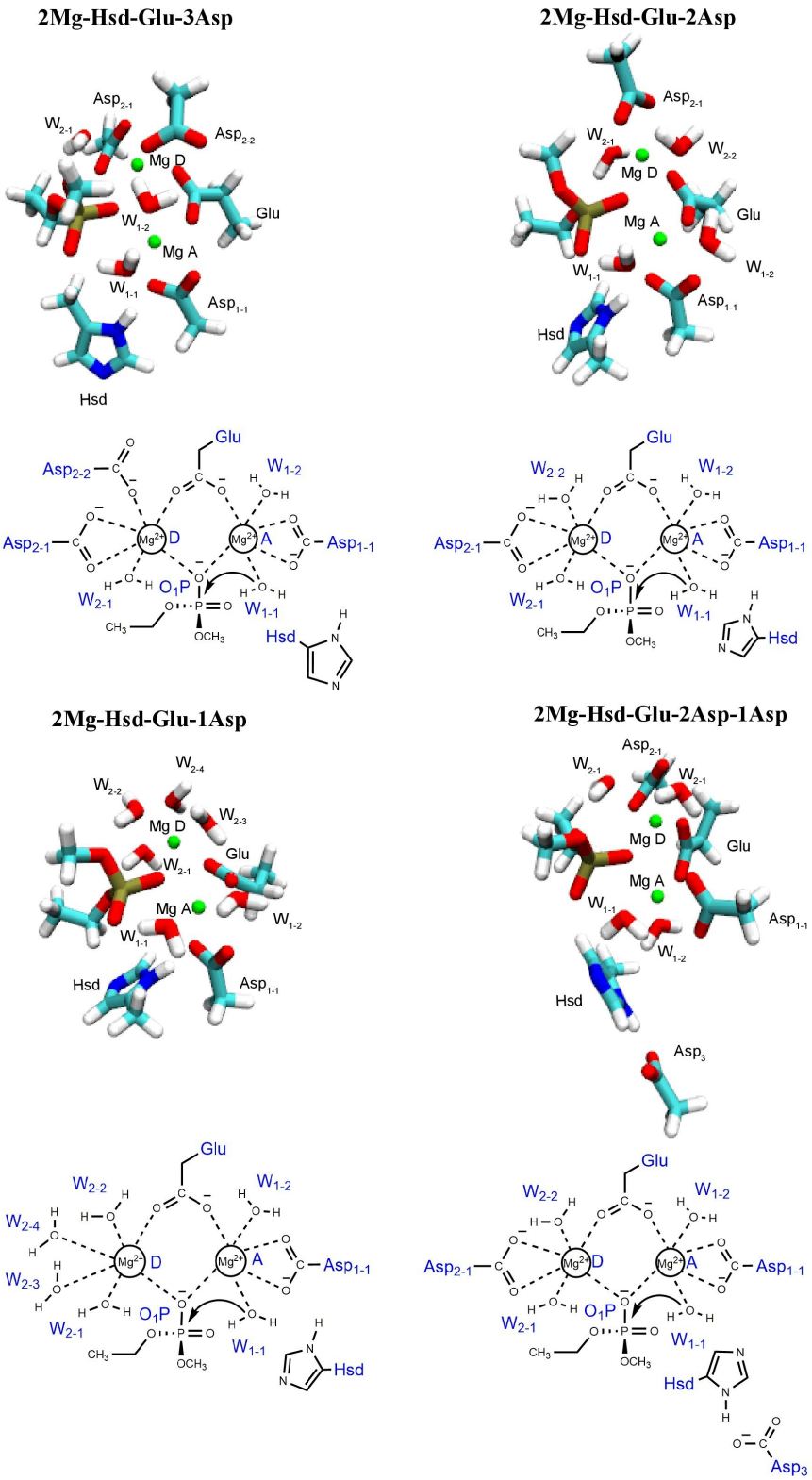

Figure 3: Reactant states for two-metal models. The scheme indicates the attack by the nucleophilic water molecule.

Table 1: List of models and mechanism analysed in his study. For the reactant states of the one-metal models (1Mg) see Figure 2 and for the two-metal models (2Mg) see Figure 3, respectively.

Model	Mechanism	Figure
1MgA-Hsp-Glu-1Asp-1Asp	1MgA-p	4
1MgD-Hsp-Glu-1Asp-1Asp	1MgD-p	5
1MgA-Hsd-Glu-1Asp-1Asp	1MgA-d	8
	1MgA-h	10
1MgD-Hsd-Glu-1Asp-1Asp	1MgD-d	9
	1MgD-h	11
2Mg-Hsd-Glu-3Asp	2Mg-d3	12
2Mg-Hsd-Glu-2Asp	2Mg-d2	13
2Mg-Hsd-Glu-1Asp	2Mg-d1	14
2Mg-Hsd-Glu-2Asp-1Asp	2Mg-h	15

anchor atoms.

All minima and transition state structures have been initially calculated using CHARMM [53] interfaced to the semi-empirical DFTB3/3OB [54] as quantum method, using specified parameter for phosphorus and magnesium [55]. Minima for reactant, product, and intermediate states were obtained with 10^{-7} a.u. as SCF convergence criterion and 10^{-4} a.u./Å as criterion for the geometry optimization. As outlined in the introduction, two extreme types of mechanisms, dissociative or associative, are possible in the cluster models. Two dimensional scans of the DFTB potential energy surface (PES) using the P–OH2 distance (nucleophilic attack) and the P–O3' distance (leaving group departure) as coordinates, have been carried out to explore whether an associative or a dissociative mechanism is more likely. The PES scans of different one-metal and two-metal models suggest an associative mechanism to be the most favorable (see Figures S1–S4 and S5–S7). Moreover, no dissociative intermediate could be trapped on the B3-LYP of theory.

We then inspected the respective associative mechanisms more closely by modeling and optimizing various intermediate states of nucleophilic attack, leaving group departure, and several proton transfer steps preceding or accompanying the P–O bond making and breaking. Minimum energy pathways between those minima have then been computed using the conjugate peak refinement (CPR) method [56] as implemented in CHARMM. Subsequently, selected minima and transitions states were refined applying the B3-LYP hybrid functional [57, 58] and the 6-31G(d,p) basis set [59] as implemented in the Gaussian 09 program package [60]. The geometry convergence criteria was tightened to 1×10^{-8}a.u./Å.

The nature of the optimized stationary points (minima or transition states) was verified by normal mode analysis. Additionally, intrinsic reaction coordinates have been followed, starting from the transition structures in both forward and backward direction, so as to validate the minima connected by the respective transition.

All optimizations have been carried out in vacuum and in implicit water, using the polarization continuum method as implemented in the Gaussian 09 with a dielectric constant of $\epsilon = 80$. Partial atomic charges were calculated on the basis of natural bond orbital (NBO) analyses [61].

Results and Discussion

One-metal models

One magnesium ion and protonated histidine: Mechanisms 1MgA-p and 1MgD-p

For the 1MgA-p mechanism computed for a model with one magnesium atom located at the attack site, protonated histidine, and one extra aspartate residue (see model 1MgA-Hsp-Glu-1Asp-1Asp in Figure 2) the barrier for nucleophilic attack (TS1_1MgA-p) is 34.9 kcal/mol in vacuum (34.8 kcal/mol in solvent) (see Figure 4). Upon this attack a proton is transferred from the water molecule to the O2P atom of the phosphate group (see Figure 6) leading to a pentacovalent intermediate, Int1_1MgA-p, with an energy about as high as the transition state leading to it (34.7 kcal/mol and 33.7 kcal/mol in vacuum and solvent, respectively). The second step of the rotates the HO2–P such that the hydrogen atom points towards the O3' atom of the leaving group. The corresponding transition state, TS2_1MgA-p, has a similar energy as the nucleophilic attack in this mechanism (34.9 kcal/mol in vacuum and 34.7 kcal/mol in solvent). Leaving group departure, coupled to a proton transfer from the phosphate O2P atom to the O3' atom, goes through the transition state with the highest energy along this 1MgA-p mechanism (40.4 kcal/mol in vacuum and 39.9 kcal/mol in solvent, respectively).

Placing the magnesium ion at the departure site (see model 1MgD-Hsp-Glu-1Asp-1Asp in Figure 2), results in a mechanism 1MgD-p with a reduced barrier of 29.0 kcal/mol (∼28kcal/mol in solvent, Figure 5) for the nucleophilic attack in . Also the pentacovalent intermediate in this mechanism, Int1_1MgD-p has a lower energy than in the 1MgA-p mechanism with the magnesium ion located at the attack site: 23.7 kcal/mol in vacuum and 24.kcal/mol in solvent, respectively.

It should be noted that the magnesium ion is coordinated by the same type and number of ligands (water molecules and amino acid residues) in both positions, i.e. on the attack and on the departure site. One difference is, however, the loss of a favourable hydrogen-bonded contact of the nucleophilic water molecule to residue Asp1 in the reactant state of mechanism 1MgA-p upon attack which is a possible explanation for the increase in activation energy compared to the 1MgD-p mechanism.

The rotation of the HO2–P group has a transition state, TS2_1MgD-p, of relative energy of

35.0 kcal/mol (34.3 kcal/mol in solvent) which is the highest point along this mechanism (cf. Figure 5). Leaving group departure in this mechanism has a transition state, TS2_1MgD-p, of similar energy (30.0 kcal/mol) as the one of the nucleophilic attack, TS1_1MgD-p.

The barriers calculated for the1MgD-p mechanism are somewhat lower than those calculated for uncatalyzed phosphodiester hydrolysis in which only the phosphate group and the nucleophilic water molecules are considered [62], or those calculated in the presence of a water-ligated magnesium ion [63]. The small catalytic effect by the additional residues in the present model (glutamate and aspartate ligating the magnesium ion, and a histidine residue) can be explained by a positioning of the nucleophile. The substantially higher barrier (40.5 kcal/mol) for P-O bond scission with a proton transfer from a metal-ligated water molecule to the O3'-atom of the leaving group renders also the catalytic effect of the magnesium ion to be structural rather than by direct participation on the reaction.

One magnesium ion and neutral histidine: Mechanisms 1MgA-d and 1MgD-d

To check whether the positive charge of the protonated histidine plays an important role in stabilizing the transition state for nucleophilic attack we computed a similar associative mechanism of a cluster model with one magnesium ion and a neutral histidine, again with the magnesium ion located on either the attack site or at the departure site (see models 1MgA-Hsd-Glu-1Asp-1Asp, and 1MgD-Hsd-Glu-1Asp-1Asp in Figure 2, respectively).

The transition state for nucleophilic attack with proton transfer from the attacking water molecule to the phosphate group has an energy of 29.6 kcal/mol in vacuum (38.6 kcal/mol in solvent) if the magnesium ion is located on the attack (Figure 8, TS1_1MgA-d) site and 35.1 kcal/mol in vacuum (39.4 kcal/mol in solvent) if the metal ion is located on the departure site (Figure 9, TS1_1MgD-d). Comparison of these energies with those obtained for the 1MgA-p and 1MgD-p mechanism for models with protonated histidine suggest a favorable role of protonated histidine for the nucleophilic attack if no metal ion is located on the attack site. In that case the barrier for nucleophilic attack is similar to the one computed for the 1MgA-p mechanism, indicating that the presence of a positive charge on the attack site is favourable for this first step. T Because of the high initial barrier no further steps have been computed for the 1MgD-d mechanism. The rate-determining step in the 1MgA-d mechanism is the cleavage of the scissile bond with a transition state energy of 39.2 kcal/mol (39.5 kcal/mol in solvent).

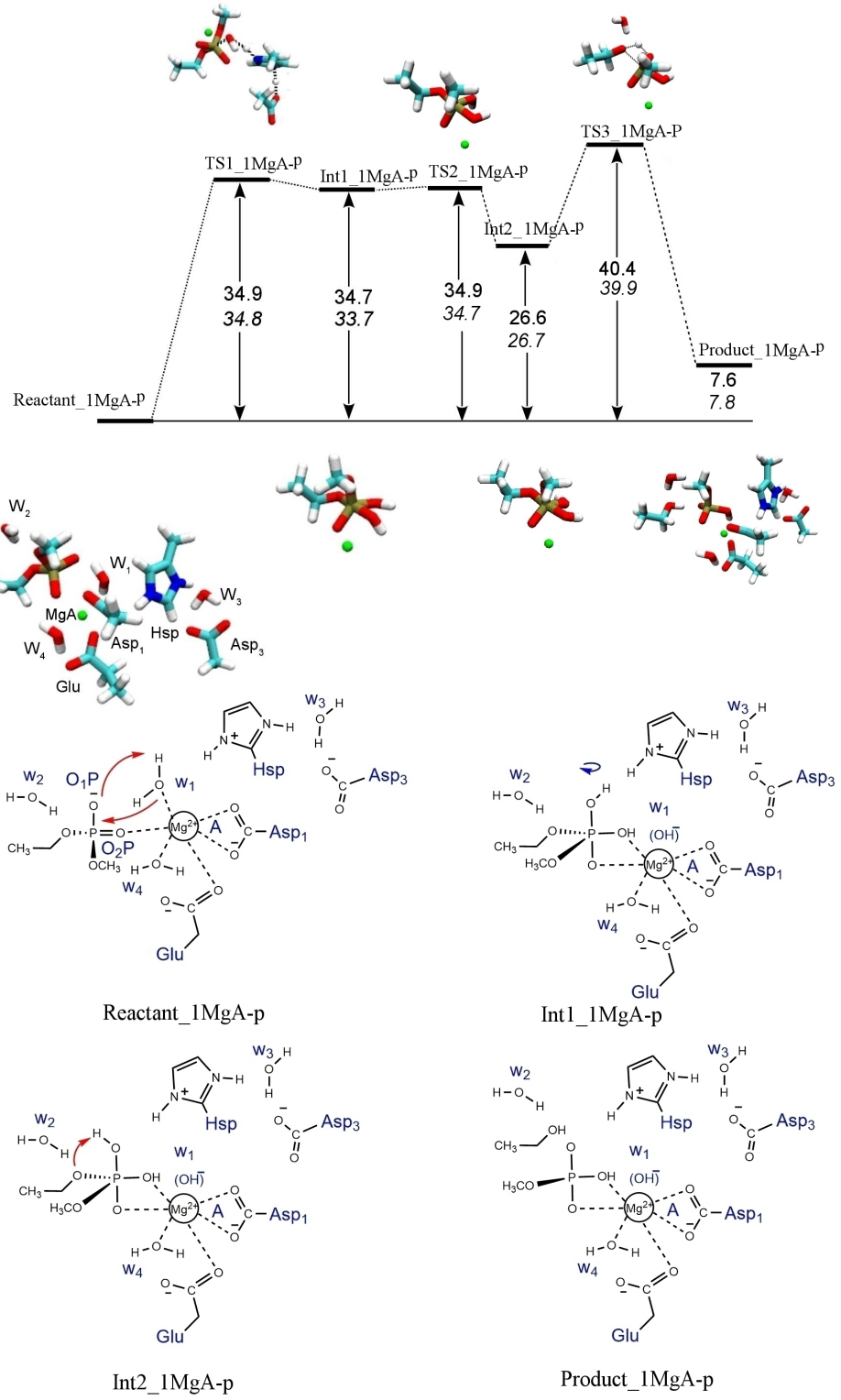

Figure 4: Mechanism, 1MgA-p, for model with one magnesium ion located a the attack site, A, and protonated histidine (see 1MgA-Hsp-Glu-1Asp-1Asp in Figure 2), calculated by B3LYP/6-31G(d,p) in vacuum (upright numbers) and solvent (in italics). All energies (in kcal/mol) are given relative to the reactant state.

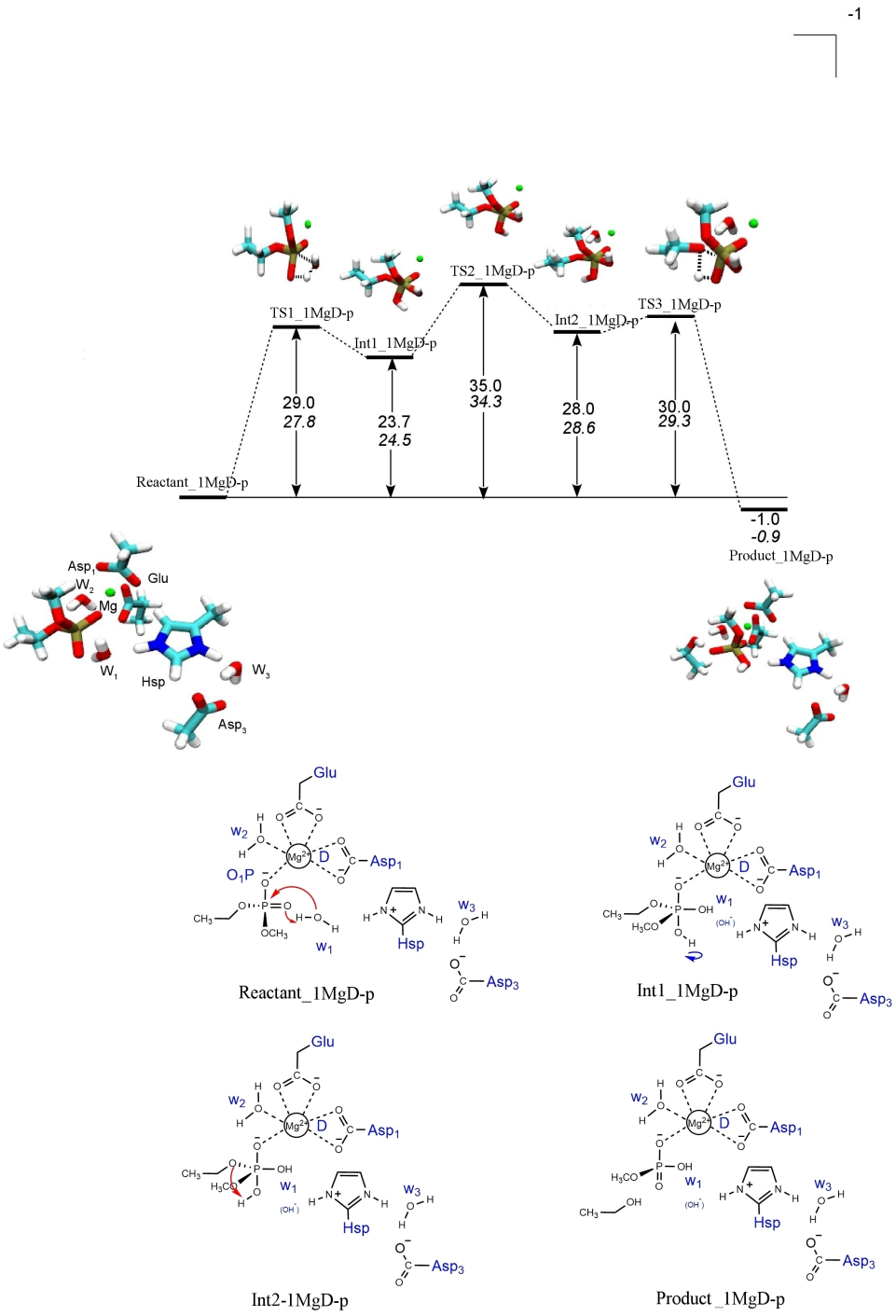

Figure 5: Mechanism,1MgD-p, for model with one magnesium ion located at the departure site, D, and protonated histidine (see 1MgD-Hsp-Glu-1Asp-1Asp in Figure 2), calculated by B3LYP/6-31G(d,p) in vacuum (upright numbers) and solvent (in italics). All energies (in kcal/mol) are given relative to the reactant state.

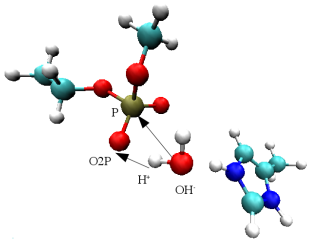

Figure 6: Attack of a water molecule on the phosphorus atom of a phosphodiester.

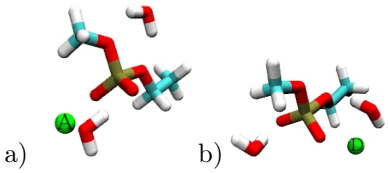

Figure 7: Different position of the magnesium ion in a) model with one magnesium ion at the attack site, A, and b) model with one magnesium ion at the departure-site, D.

One magnesium ion and neutral histidine: Mechanisms 1MgA-h and 1MgD-h

Another possibility to activate the water molecule for nucleophilic attack is the transfer of a proton to the Nδ atom of the unprotonated histidine residue. In the corresponding models (see 1MgA-Hsd-Glu-1Asp-1Asp and 1MgD-Hsd-Glu-1Asp-1Asp in Figure 2), the aspartate mimic is positioned close to the histidine, forming a hydrogen bond to the Nϵ atom. This conformation resembles a catalytic triad [64, 65] (if the nucleophile is included) that allows shuttling of a proton between histidine and aspartate, thus facilitating acceptance of a proton from the nucleophilic water molecule.

Indeed, a significant reduction in the energy barrier can be observed in such a histidine-assisted nucleophilic attack, dropping to 23.5 kcal/mol (25.4 kcal/mol in solvent) in the 1MgA-h mechanism (Figure 10, TS1_1MgA-h) and to 27.4 kcal/mol (26.2 kcal/mol, in solvent) in the 1MgD-h mechanism (Figure 11, TS1_1MgD-h) . In the latter model, this is the rate determining step in this mechanism (Figure 11). In the resulting intermediate, Int1_1MgD-h, the scissile bond is already cleaved, thus proton transfer, nucleophilic attack and leaving group departure all take place in one step. The remaining reprotonation steps have negligible barriers.

In contrast, in the mechanism calculated for a model with the metal ion located on the attack site, 1MgA-h, nucleophilic attack and leaving group departure are separate steps, indicating some stabilization of the pentacovalent intermediate, Int1_1MgA-h, by the metal ion. In fact, leaving group departure is preceded by proton transfer from the histidine to the phosphate group (TS2_1MgA-h with 28.3 kcal/mol barrier in vacuum and 31.1 kcal/mol barrier in solvent, respectively). The final cleavage of the scissile bond, assisted by proton transfer from a magnesium-bound

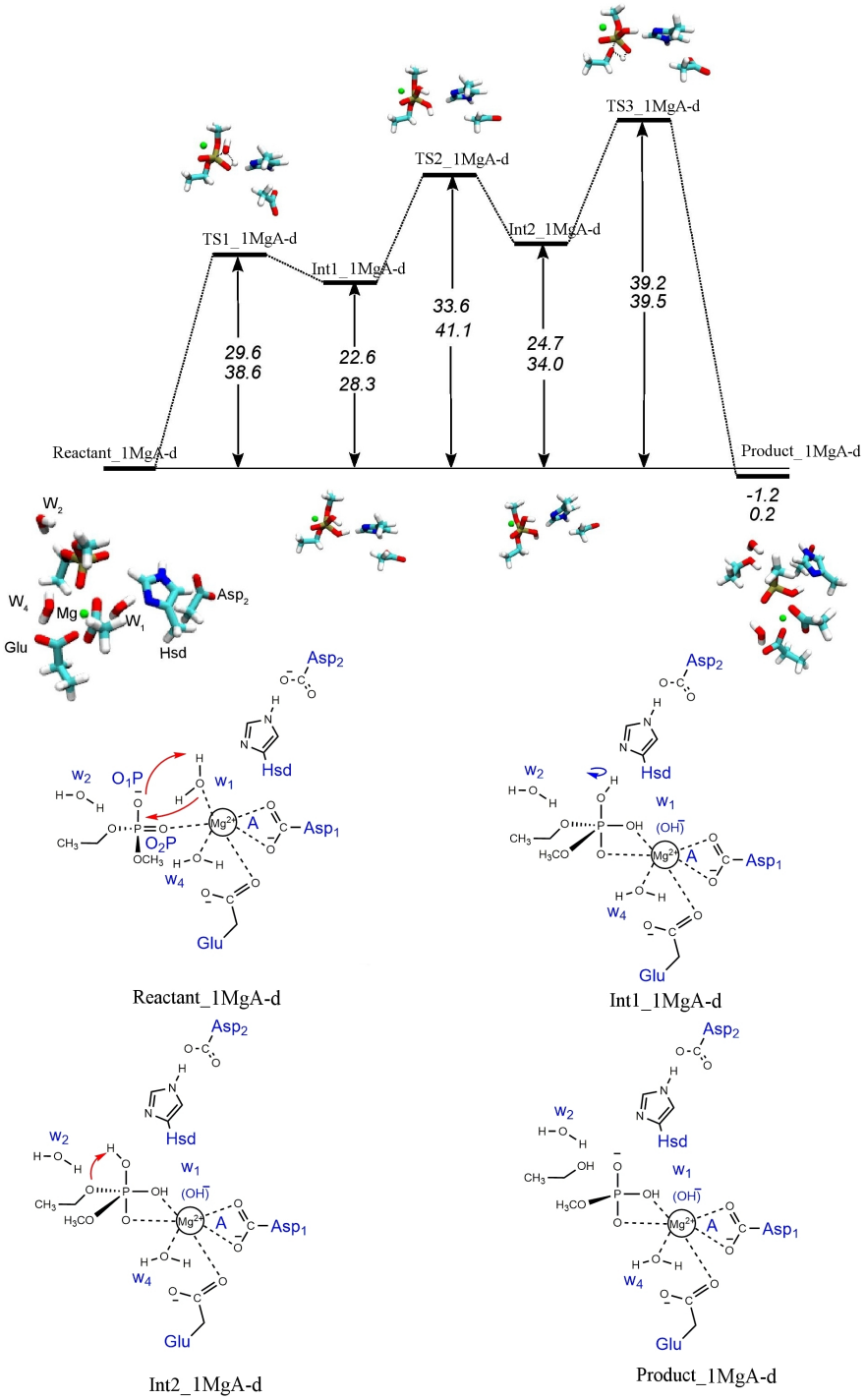

Figure 8: Direct mechanism, 1MgA-d, in the model with one magnesium located at the attack site, neutral histidine, and two aspartate residues (see 1MgA-Hsd-Glu-1Asp-1Asp in Figure 2), calculated by B3LYP/6-31G(d,p) in vacuum (upright numbers) and solvent (in italics). Energies (in kcal/mol) are given relative to the reactant state.

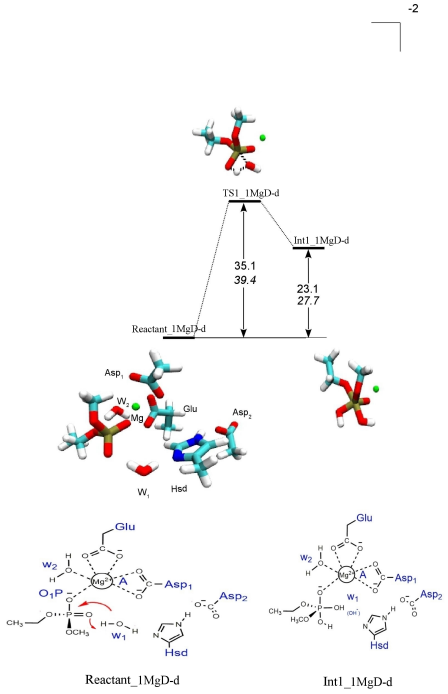

Figure 9: Direct nucleophilic attack, 1MgD-d, in the model with one magnesium ion located at the departure site, neutral histidine, and two aspartate residues, (see 1MgD-Hsd-Glu-1Asp-1Asp in Figure 2), calculated by B3LYP/6-31G(d,p) in vacuum (upright numbers) and solvent (in italics). Energies (in kcal/mol) are given relative to the reactant state.

water molecule, has a transition state energy of 39.2 kcal/mol (39.5 kcal/mol in solvent) and is the rate determining step like in the 1MgA-d mechanism. These rate-determining barriers for leaving group departure are close to those of uncatalyzed dimethyl-phosphate hydrolysis [14]. This is reasonable since the magnesium ion situated on the "attack site" does not have a proper catalytic effect on leaving group departure.

Table 2: Energies of stationary points along the most favourable phosphate hydrolysis mechanisms computed for the one-metal models. All energies (in kcal/mol) have been calculated with (B3LYP, 6-31G(d,p)) and are given relative to the respective reactant state.

Mechanism	TS1	Int1	TS2	Int2	TS3	Int3	TS4	Product
1MgA-p vacuum	34.9	34.7	34.9	26.6	40.4			7.6
1MgA-p solvent	34.8	33.7	34.7	26.7	39.9			7.8
1MgD-p vacuum	29.1	23.7	35.0	28.0	30.0			-1.0
1MgD-p solvent	31.3	26.7	36.2	29.0	31.5			-0.7
1MgA-d vacuum	29.6	22.6	33.6	24.7	39.2			-1.2
1MgA-d solvent	38.6	28.3	41.1	34.0	39.5			0.2
1MgA-h vacuum	23.5	23.3	28.3	22.6	33.6	24.7	39.2	-1.2
1MgA-h solvent	25.4	25.0	31.1	28.3	41.1	34.0	39.5	0.2
1MgD-h vacuum	27.4	-2.61	22.8	-4.7	-4.3			-6.1
1MgD-h solvent	26.2	-1.4	14.22	-4.6	-2.3			-2.6

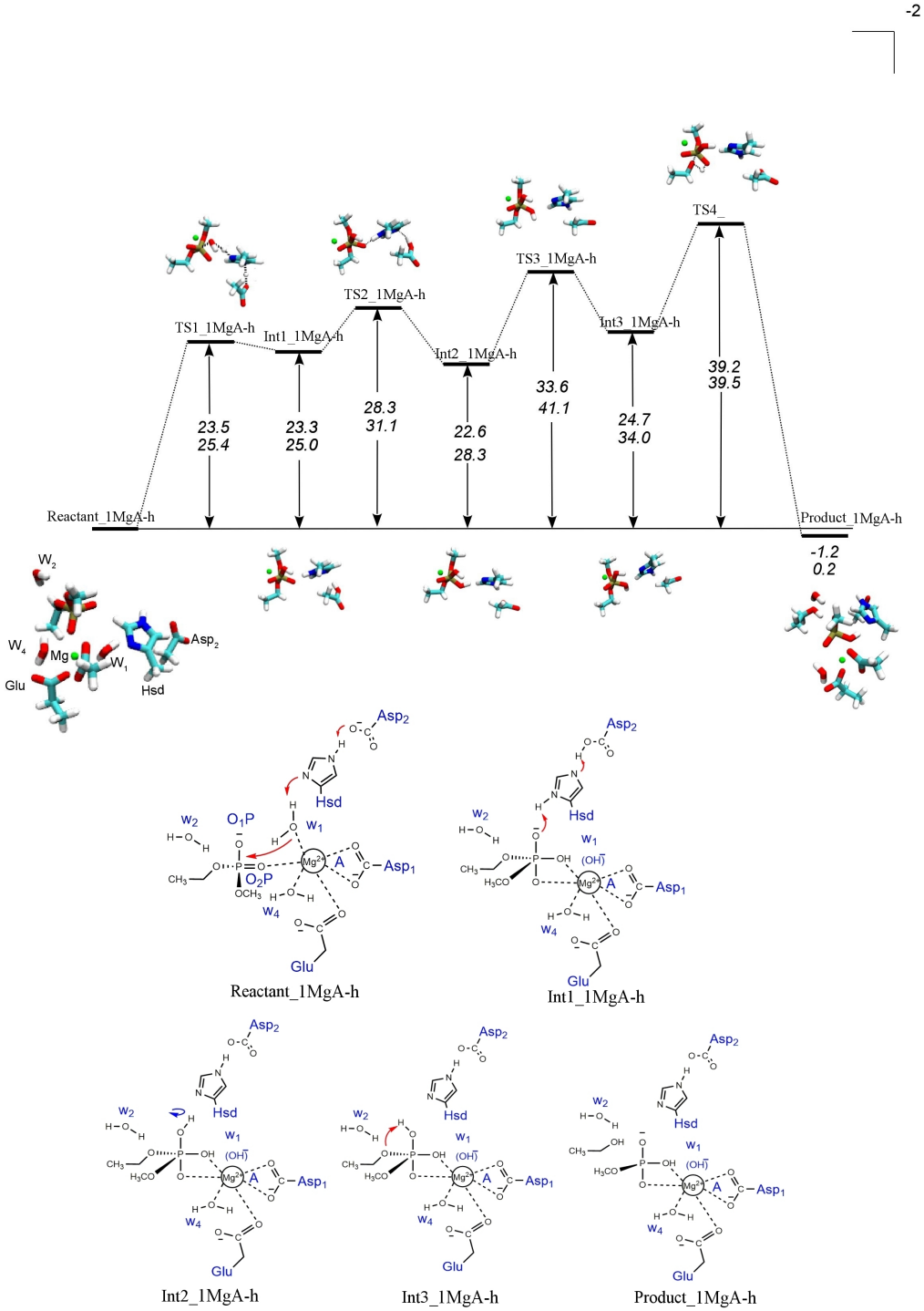

Figure 10: Histidine-assisted mechanism (1A-h) for model with one magnesium ion located at the attack site, neutral histidine and two aspartate residues, 1MgA-Hsd-Glu-1Asp-1Asp, calculated by B3LYP/6-31G(d,p) in vacuum (upright numbers) and solvent (in italics). All energies (in kcal/mol) are given relative to the reactant state.

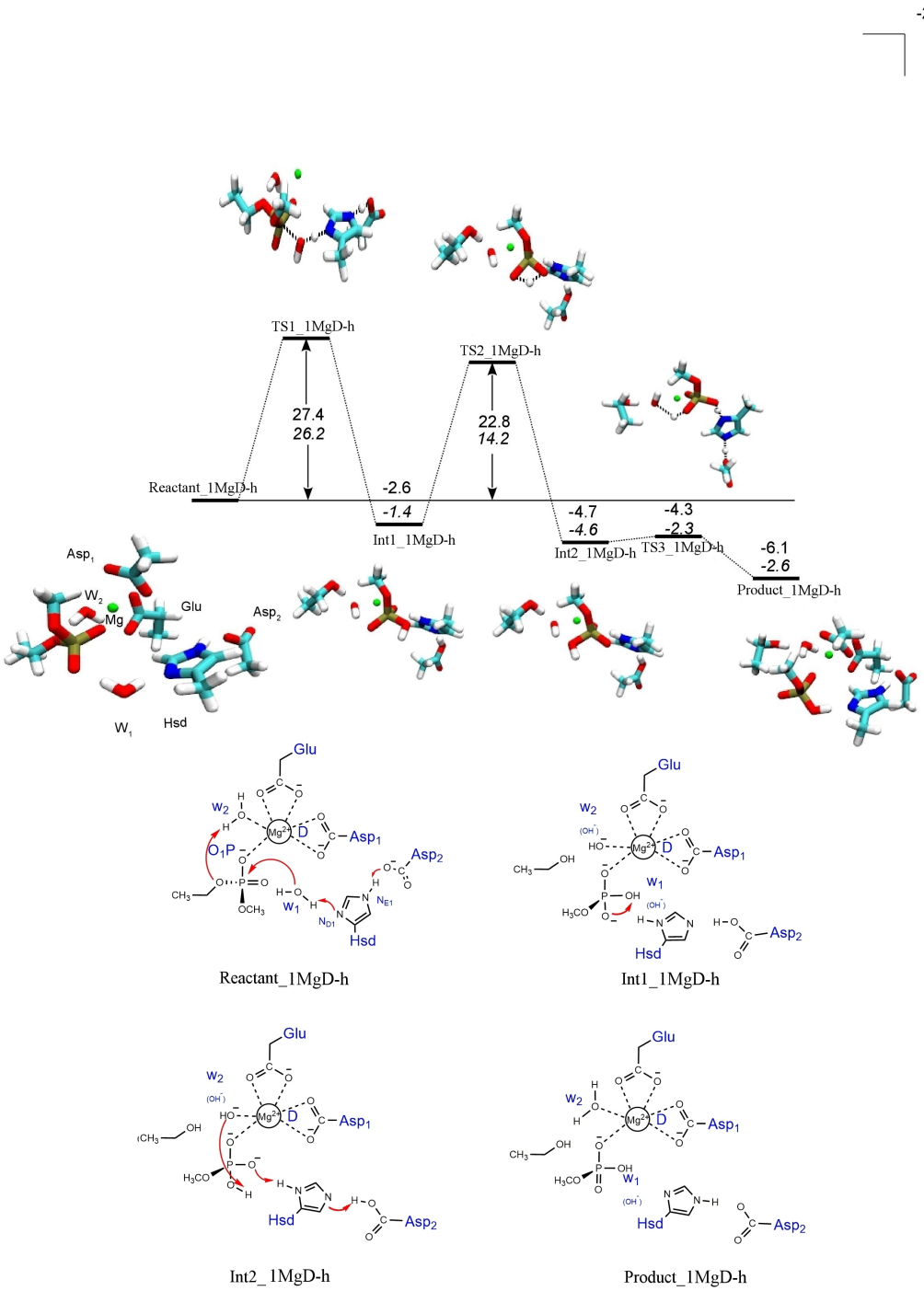

Figure 11: Histidine-assisted mechanism (1D-h) for model with one magnesium ion located at the departure site, neutral histidine and two aspartate residues, 1MgD-Hsd-Glu-1Asp-1Asp, calculated by B3LYP/6-31G(d,p) in vacuum (upright numbers) and solvent (in italics). All energies (in kcal/mol) are given relative to the reactant state..

Two-metal models

According to the potential energy scans (Figure S5–S7), also the two-magnesium models exhibit associative mechanisms for phosphate hydrolysis. Also for these models, no dissociative intermediate could be trapped on the B3LYP/6-31G(d,p) level of theory.

In the two-magnesium models, one of the two metal ions, MgA is situated on the "attack site", that is the site on which the nucleophile is located, and the second metal ion, MgD is located on the "departure site", i.e. closer to the O3' atom of the leaving group. Each metal ion is coordinated by an aspartate residue and one water molecule, a shared oxygen atom of the phosphate group, one of the two oxygen atoms of a glutamate residue, and double-coordinated by one aspartate residue (see Figure 3).

Two magnesium ions, neutral histidine and one, two, or three aspartate residues: Mechanisms 2Mg-d0, 2Mg-d1, and 2Mg-d2

To test whether an increase in positive charge on the "departure site" has an activating effect on the leaving group, we have setup models in which the second metal ion is coordinated by two, one, or no aspartate residue (see models 2Mg-Hsd-Glu-3Asp, 2Mg-Hsd-Glu-2Asp, and 2Mg-Hsd-Glu-1Asp in Figure 3). The corresponding to mechanisms are termed 2Mg-d2, 2Mg-d1, and 2Mg-d0, respectively.

For these direct mechanisms in the two-metal models the energy barriers for nucleophilic attack (26.0 kcal/mol in vacuum and 26.6 kcal/mol in solvent, 22.5 kcal/mol in vacuum and 22.4 kcal/mol in solvent, and 29.2 kcal/mol in vacuum and 29.1 kcal/mol in solvent for TS1_2Mg-d2, TS1_2Mg-d1, and TS1_2Mg-d0, respectively) do not show any trend with respect to the total charge of the system with hardly any difference between vacuum and solvent models. Moreover, these energy barriers are similar to the barrier computed for the histidine-activated nucleophilic attack in the one-metal mechanism 1MgD-h (TS1_1D-h 27.4 kcal/mol in vacuum and 26.2 kcal/mol in solvent. respectively) and the one-metal 1MgD-p mechanism with protonated histidine (TS1_1MgD-p 29.0 kcal/mol in vacuum and 27.8 kcal/mol in solvent, respectively). In the latter, as well as in this two-metal model, one proton of the nucleophilic water molecule is directly transferred to an oxygen atom of the phosphate group and the remaining OH^- ion attacks to the phosphorous atom (Figure 12 and 5).

In all these cases, generation of an OH^- ion can be regarded as favored by the nearby residues: the positive charge of the histidine or the magnesium ion "push" the proton from the nucleophile towards the phosphate and/or stabilize the negatively charged hydroxide ion. In the histidine-

assisted mechanism, the proton is ultimately accepted by the aspartate residue at the end of the triad.

An impact of the charge difference due to another aspartate residue on phosphate hydrolysis can, however, be seen in the reaction energies in vacuum which are 3.2 kcal/mol in the 2Mg-d2 mechanism as opposed to the exothermic reaction in the 2Mg-d1 mechanism with -6.0 kcal/mol relative product energy. This effect is not observed in solvent where the reaction energies, -3.3 kcal/mol and -2.2 kcal/mol in the 2Mg-d2 and 2Mg-d1 mechanism, respectively, are rather similar, indicating that the additional negative charge introduced by an aspartate residue, is screened in solvent.

The computed direct reaction pathways for the two-metal models, 2Mg-d2, 2Mg-d1, and 2Mg-d0, show no significant difference in the energy barrier for departure of the leaving group which is the rate-determining step in all these mechanisms (with 37.6 kcal/mol, 32.0 kcal/mol and 32.1 kcal/mol in vacuum, and 34.3 kcal/mol, 34.9 kcal/mol, and 34.1 kcal/mol in solvent, respectively, and see also Table 3) In the 2Mg-d3 mechanism the transition state energy for this step is even higher than the respective transition state energies in all the one-metal mechanisms calculated in this work. Therefore, the second magnesium ion near the O3' likely does not play a catalytic role in leaving group departure.

Dissociation of the scissile bond in the pentacovalent intermediate is accompanied by a proton transfer from the O2P atom of the phosphate group to the leaving group. This proton can alternatively be transferred from a metal-ligated water molecule. In all models studied here, the energy barriers for the latter option, leaving group departure with accepting a proton from a metal-ligated water molecule, (47.5 kcal/mol, 37.8 kcal/mol and 38.5 kcal/mol for 2Mg-d2, 2Mg-d1, and 2Mg-d0, respectively) are higher than than those for leaving group departure with a proton transfer from the O2P atom. This preference for the proton transfer from the O2P atom can be explained by the metal-bound phosphate group being a stronger Bronsted acid, i.e. a better proton donor than a metal-activated water molecule.

Two magnesium ions, neutral histidine and three aspartate residues: Mechanism 2Mg-h

In order to calculate a histidine-assisted mechanism similar to those obtained for the one-metal models, 1MgA-h and 1MgD-h,(Figures 10 and 11), we placed the third aspartate residue in hydrogen-bond distance to the histidine (see model 2Mg-Hsd-Glu-2Asp-1Asp in Figure 3). Direct attack of the water molecule with proton transfer to the phosphate group in this model has a barrier of 29.5 kcal/mol (25.4 kcal/mol in solvent) ad is thus comparable to the direct nucleophilic

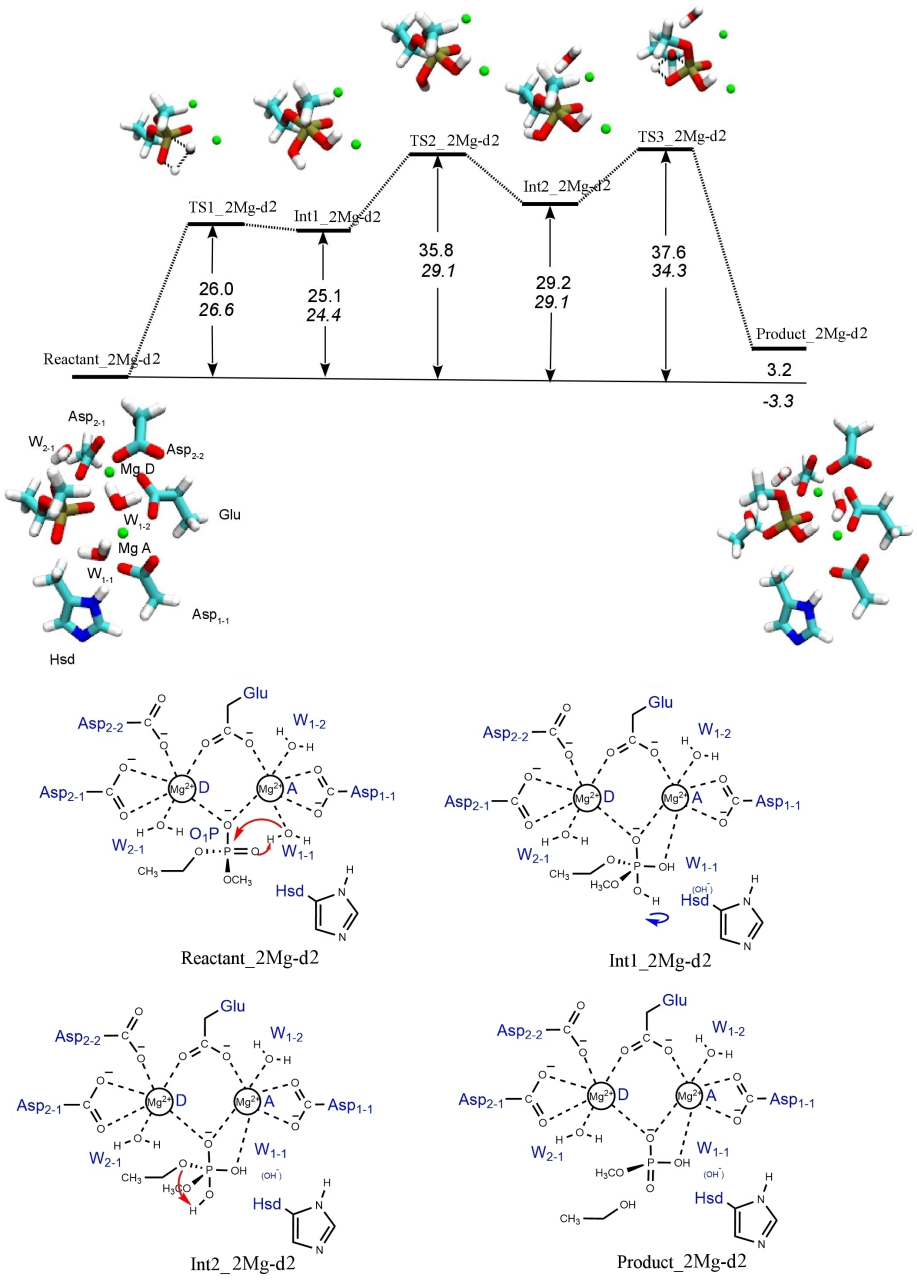

Figure 12: Mechanism 2Mg-d2 for model with two magnesium ions, neutral histidine, and three aspartate residues (see 2Mg-Hsd-Glu-3Asp in Figure 3), calculated by B3LYP/6-31G(d,p) in vacuum (upright numbers) and solvent (in italics). Energies (in kcal/mol) are given relative to the reactant state.

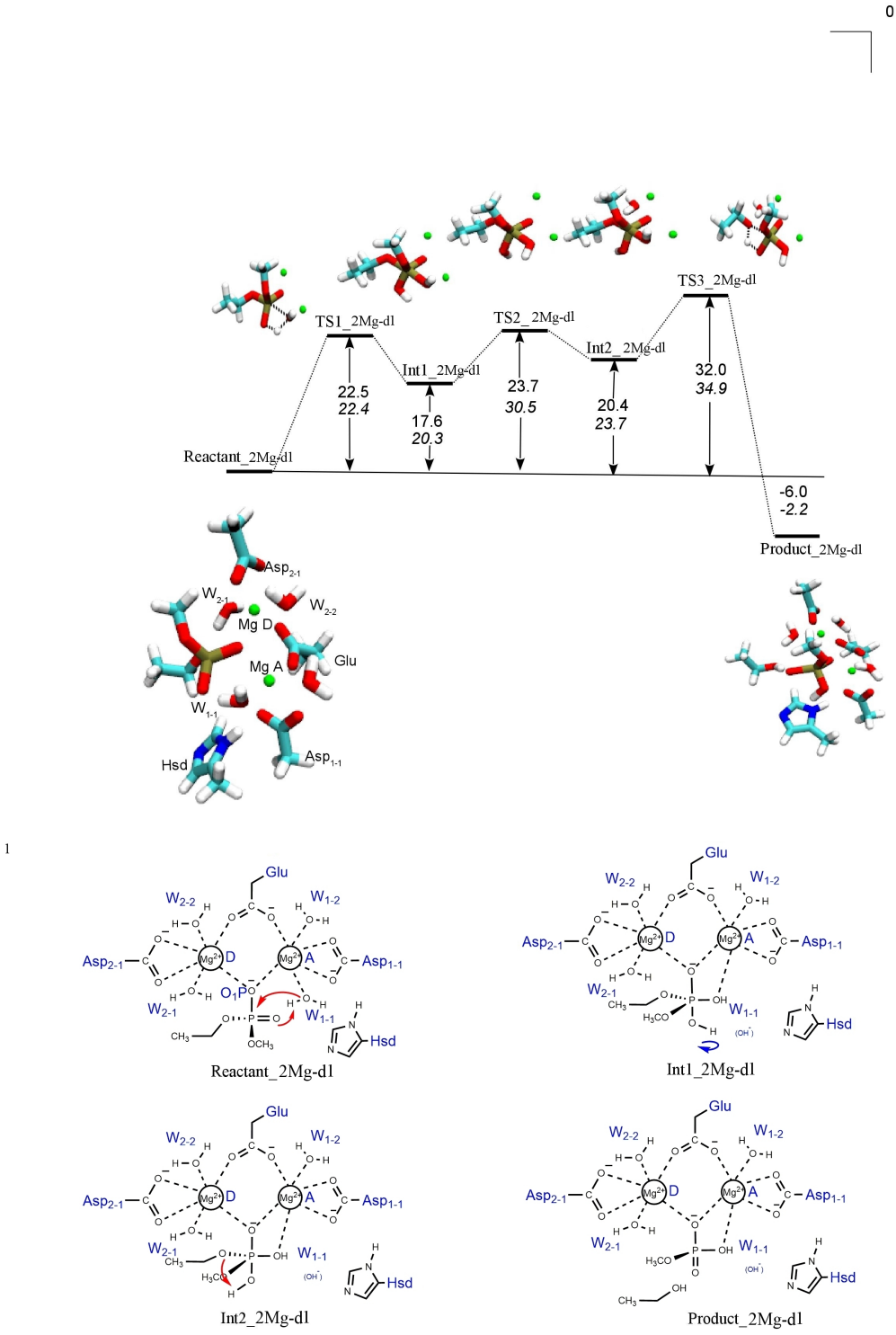

Figure 13: Mechanism 2Mg-d1 for model with two magnesium ions, neutral histidine, and two aspartate residues (see 2Mg-Hsd-Glu-2Asp in Figure 3), calculated by B3LYP/6-31G(d,p) in vacuum (upright numbers) and solvent (in italics). All energies are in kcal/mol relative to the reactant state.

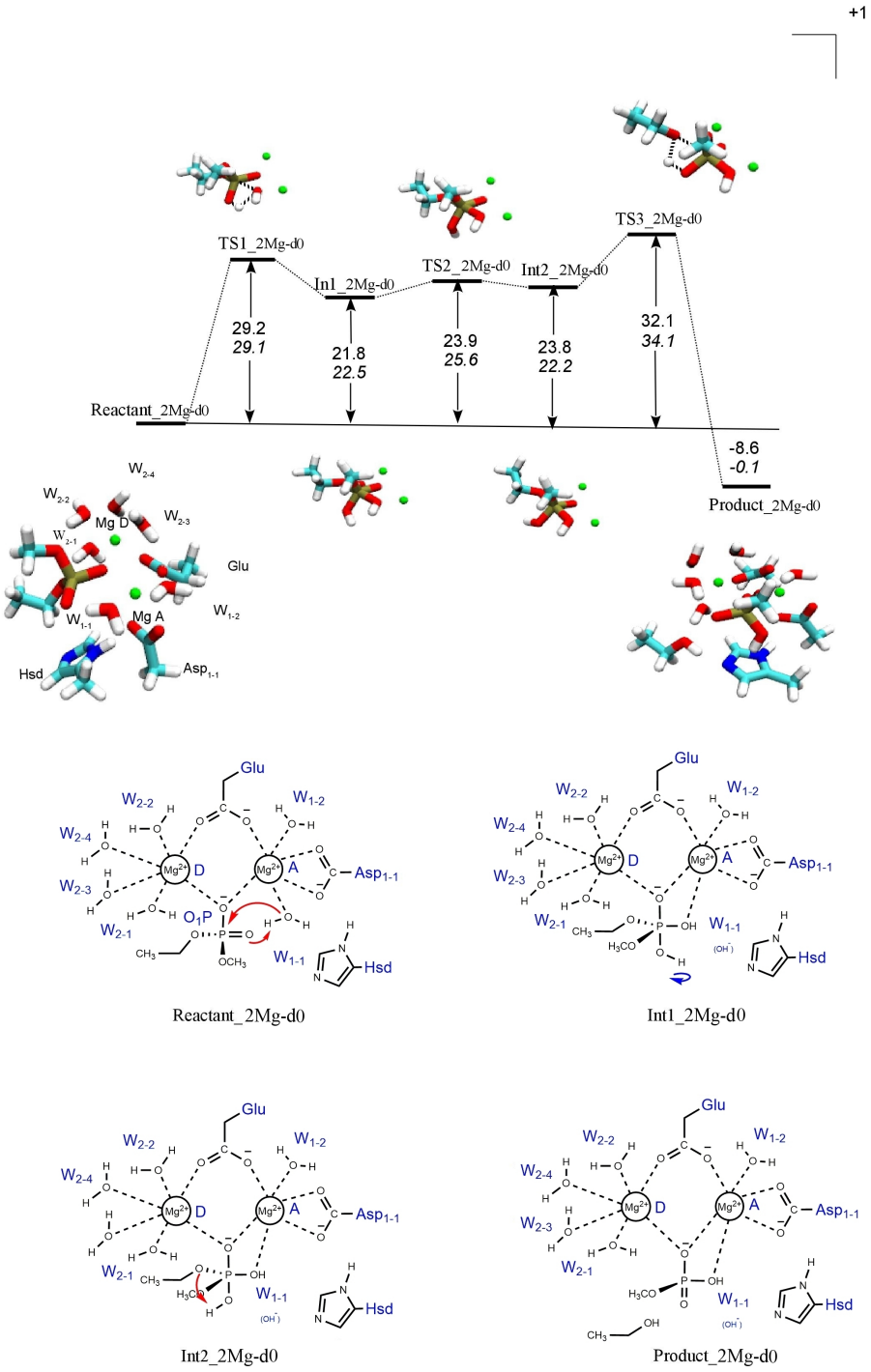

Figure 14: Mechanism 2Mg-d0 for model with two magnesium ions, neutral histidine, and one aspartate residue (see 2Mg-Hsd-Glu-1Asp in Figure 3), calculated by B3LYP/6-31G(d,p) in vacuum (upright numbers) and solvent (in italics). All energies are in kcal/mol relative to the reactant state

attack in the other two-metal models..

In contrast, the mechanism with shuttling a proton from the nucleophilic water molecule to the Nϵ atom of the histidine, 2Mg-h, has an energy barrier for nucleophilic attack that is reduced to 9.7 kcal/mol (16.9 kcal/mol in solvent). The second transition state for dissociation of the scissile bond is 12.1 kcal/mol (18.6 kcal/mol in solvent) and thus also considerably lowered compared to the leaving group departure steps in the other two-metal models as well as lower than in the histidine-activated mechanism of the one-magnesium models (1MgA-h and 1MgD-h). The rate determining step in the 2Mg-h mechanism is the final proton transfer from the Nϵ atom of the histidine residue to the dissociated alcohol. The transition energy for this proton transfer step is 25.8 kcal/mol (29.2 kcal/mol in solvent). This rather high energy barrier is still the lowest rate-determining barrier among all mechanisms and vacuum models studied in this work. In solvent, the barrier for this reprotonation step is comparable or slightly higher than the ones computed for nucleophilic attack of the other models. The barriers for the nucleophilic attack and dissociation of the scissile bond, however, are significantly lower than in all other models and mechanisms proposed in this work.

Table 3: Energies of stationary points along the phosphate hydrolysis mechanisms computed for the two-metal models (2Mg). All energies are given in kcal/mol, relative to the respective reactant state.

Model	TS1	Int1	TS2	Int2	TS3	Int3	TS4	Product
2Mg-d2 vacuum	26.0	25.1	35.8	29.2	37.6			3.2
2Mg-d2 solvent	26.6	24.4	29.1	29.1	34.3			-3.3
2Mg-d1 vacuum	22.5	17.6	23.7	18.3	32.0			-6.0
2Mg-d1 solvent	22.4	20.3	30.5	23.7	34.9			-2.2
2Mg-d0 vacuum	29.2	21.8	23.9	23.8	32.1			-8.6
2Mg-d0 solvent	29.1	22.5	25.6	22.2	34.1			-0.1
2Mg-h vacuum	4.4	0.3	9.7	8.2	12.1	-3.7	25.8	-5.2
2Mg-h solvent	8.1	7.2	16.9	15.6	18.6	1.7	29.2	-3.5

Comparison to other studies of phosphate hydrolysis in cluster models and in enzymes

In all models with two magnesium ions, both MgA and MgD share their positive charge with the phosphate group via the O1P atom. In these models a catalytic effect on the nucleophilic attack,

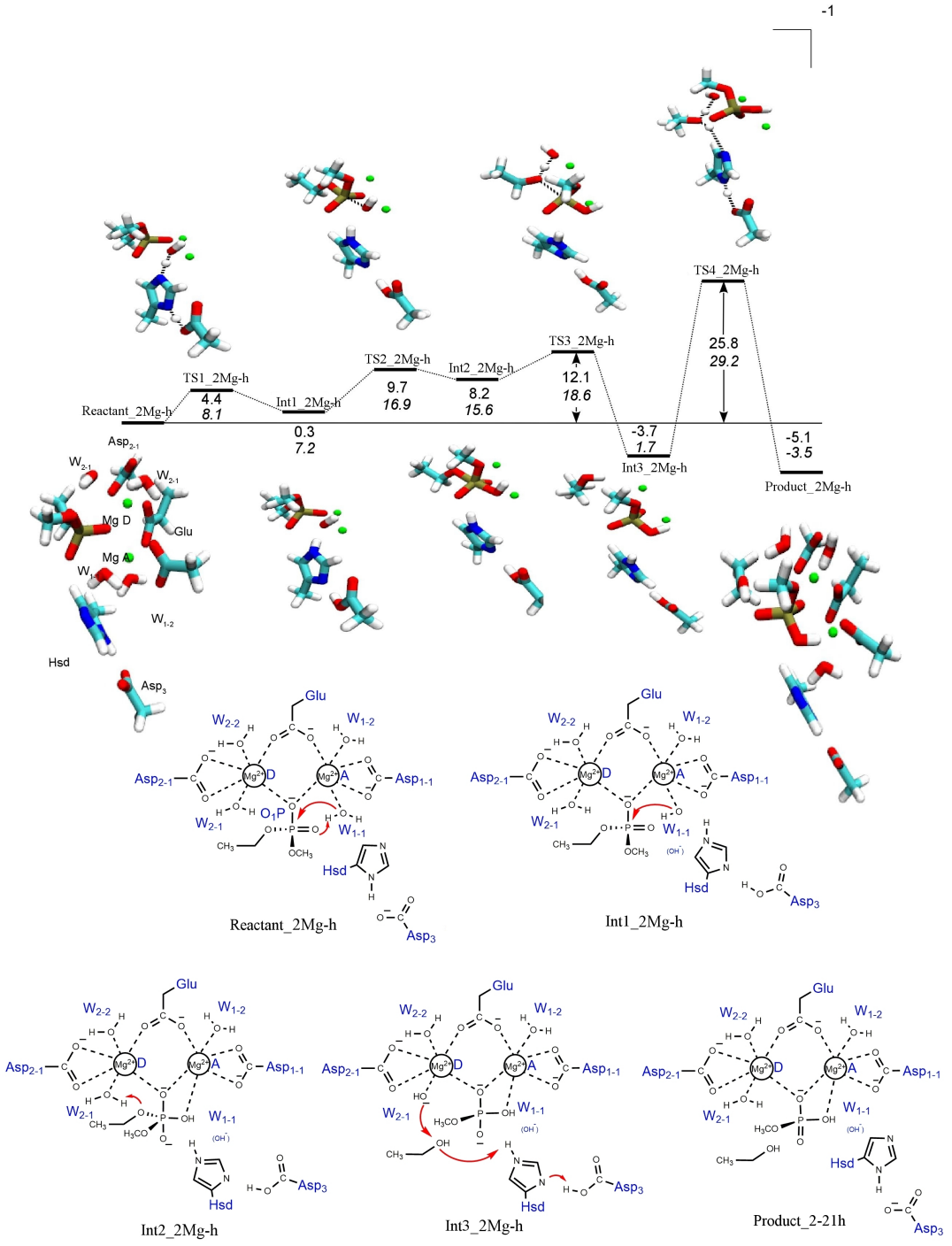

Figure 15: Histidine-assisted mechanism, 2Mg-h, for model with two magnesium ions, neutral histidine, and three aspartate residues (see 2Mg-Hsd-Glu-2Asp_1Asp in Fig. 3) calculated by B3LYP/6-31G** in vacuum (upright numbers) and solvent (in italics). All values are in kcal/mol relative to the reactant state.

likely through balancing the increasing negative charge, can be observed. Our computed reaction pathways show transferring a proton to the O2P atom of the phosphate group together with attack of the nucleophile to have barriers that are significantly reduced compared to the Gibbs free energy (38 kcal/mol) computed for dimethyl phosphate hydrolysis without any surrounding amino acid residues or metal ions [16]. In that study the energy barrier was dissected into 19.6 kcal/mol for proton transfer from a water molecule to the O2P atom and 18.4 kcal/mol for the attack of the remaining hydroxide ion. The reduced barriers for the direct attack of the nucleophile with concerted proton transfer to the phosphate group in the cluster models is likely a consequence of a facilitated nucleophilic attack due to the close presence of an extra positive charge.

In the histidine-assisted mechanism the attack of the hydroxide ion then has an even lower barrier (only 9.7 kcal/mol in vacuum and 16.7 kcal/mol in solvent). Also in the one-metal models, histidine-assisted nucleophilic attack shows barriers that are significantly lower than those computed for direct attack. In the one-metal model, however, proton transfer for nucleophile generation, nucleophilic attack and leaving group dissociation take place in a concerted step without a pentacovalent intermediate. The barrier for this step ($\sim$27 kcal/mol) is significantly higher than the nucleophilic attack in the two-metal mechanism ($\sim$10 kcal/mol in vacuum and $\sim$17 kcal/mol in solvent, respectively), suggesting a less stabilized transition state with only one metal ion.

According to the natural bond (NBO) analysis, the negative charge on the phosphate group increases in the pentacovalent structure to such an extend (see Figure 16) that the scissile bond is cleaved without any further transition state in the one-metal model with the magnesium ion located at the departure site. In the one-metal model with the magnesium located at the attack site, however, the pentacovalent intermediate is stabilized and the leaving group departure appears not to be facilitated and does not occur spontaneously (see Figure 16). In the two-metal model, the negative charge is somewhat compensated by the second metal ion, resulting in a stable pentacovalent intermediate and another transition state for P–O3' bond dissociation with an energy of 12.1 kcal/mol. Calculations of the two-metal histidine-assisted mechanism with a solvent model show an increased barrier for proton transfer to the histidine-aspartate cluster and an intermediate that is about 7 kcal/mol higher in energy than in vacuum. The following transition states and intermediates for nucleophilic attack and leaving group departure are similarly higher in solution than in vacuum, with the leaving group departure showing an energy barrier of 18.6 kcal/mol in solvent.

Phosphate hydrolysis by the attack of a hydroxide ion and the difficulty to calculate this step and hydroxide generation accurately has been discussed in the literature where different reaction rates and types of mechanisms, stepwise or concerted fashion, have been proposed [66–69]. The

higher energies calculated for the transition states and intermediates of hydroxide generation by proton transfer to the histidine and subsequent attack with the hydroxide ion as the nucleophile computed in implicit solvent are an indicator for an artifact in the vacuum model: Neutralization of the aspartate residue that is located at the outer part of the cluster model is, in vacuum, preferable than maintaining a neutral water molecule. As suggested by the higher energies in implicit solvent, charge screening effects counteract this preference. The situation may yet be different in explicit solvent or a heterogeneous protein environment with many other charged residues. The present cluster models likely underestimate the barriers for the hydroxide generation but arguably do this in a similar fashion for all mechanisms calculated. The histidine-assisted generation of a hydroxide ion and the subsequent phosphate hydrolysis by attack of this nucleophile is therefore the most probable reaction pathway computed for the cluster models.

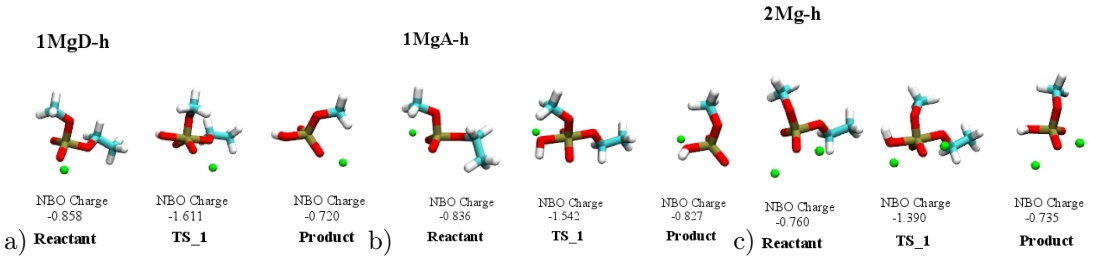

Figure 16: NBO charge (in a.u.) on the phosphate group at different steps of the histidine-assisted reaction pathway in a) one-metal model 1MgD-h, b) one-metal model 1MgA-h, and c) two-metal model 2Mg-Hsd-Glu-2Asp-1Asp .

In the histidine-assisted mechanisms, both for the one-metal and the two-metal model, the leaving group receives a proton from a metal-ligated water molecule due to the lack of a proton on the O2P atom. The barrier for the re-protonation, i.e. proton transfer from the histidine-aspartate cluster via the leaving group to that water molecule, is calculated to be the highest barrier in the histidine-assisted pathway of the two-metal model (∼25 or ∼29 kcal/mol in vacuum and solvent, respectively). It is however, conceivable that such re-protonation steps occur via additional water molecules and with much reduced barriers in a real solvent or in an enzymatic environment. Indeed, many previous mechanistic studies on cleavage of the phosphodiester employing QM/MM methods, and hence taking into account the protein environment, re-protonation steps are computed with lower barriers than the rate-determining nucleophilic attack or leaving group departure steps [25–29, 70]. Disregarding, the reprotonation step, the remaining barrier of ∼19 kcal/mol for the energetically most favorable mechanism is comparable to rates of seconds to minutes as reported for several DNA cleaving enzymes [50, 71–75]. It is significantly lower than uncatalyzed phosphate hydrolysis [15] and also lower than the phosphate hydrolysis by the direct attack of a hydroxide ion on a phospho-diester [76].

Our models, moreover, have a considerable resemblance with the nuclease domain (Nuc) of 3´hExo complexed with rAMP: two magnesium ions are coordinated by three aspartate residues and one glutamide residue together with one neutral histidine residue which is well located for accepting a proton from a hydrolytic water molecule [77]. This combination of amino acids and metal ligated water molecules offer a catalytic platform for hydrolytic cleavage of bound RNA [77]. Escherichia coli exonuclease III (ExoIII)-like apurinic/apyrimidinic (AP) endonuclease is discussed to start the reaction with the nucleophilic attack of an activated water molecule to phosphate group [78](cf. Figure1). In a proposed mechanism [79], an aspartate residue positioned close to a histidine aids in stabilizing the development of positive charge on the histidine after proton abstraction from a water molecule.

A histidine-assisted mechanism has also been proposed for endonucleolytic DNA cleavage by the homing endonuclease I-PpoI [50]. For that enzyme, however, a single magnesium ion is suggested to activate a water for donation of a proton to the O3' atom of the leaving group.

Serratia endonuclease is a magnesium dependent nuclease that is similar to I-PopI in its active site, containing a conserved histidine, likely playing the same role for activating the nucleophilic water [51]. In addition, glutamide and asparagine residues are present for binding the metal ion in both enzymes [80].

The similar composition of our cluster models, which are, of course, inspired by the enzymatic active sites, the resulting similarity in the computed most favourable mechanism and the corresponding reaction barrier in the model with experimental, enzymatic values, suggests the active site architecture to be the dominant factor in enzymatic phosphate hydrolysis. Fixing of anchor atoms in our models ensures that the residues of which the models are composed remain positioned as intended, but thereby the flexibility that can be found in an enzymatic active site cannot be mimicked properly. Furthermore, comparison of the reaction barriers for the chemical steps, however, ignores substrate binding (and product release) into the correct position which is an important factor in enzymatic reactions. In this light our results underline the importance of an enzymatic active site architecture in the catalytic reaction, given the substrate is properly positioned.

As a side-effect, we were able to evaluate the semi empirical method DFTB3/3OB [54] by comparison of reaction pathways calculating in different cluster models with the same reaction pathways calculations on the DFT level of theory (B3LYP/6-31G(d,p)). Comparison of the obtained mechanisms and barriers (see Supplementary material) obtained by DFT and DFTB for the minimalistic (cluster) models may nominate DFTB with reasonable accuracy and computational cost as a potential candidate for quantum method in hybrid QM/MM (quantum mechanics/molecular mechanics) approaches for phosphodiester hydrolysis in an enzymatic environment.

Conclusions

The phosphate hydrolysis mechanisms computed in differently composed cluster models reveal no significant catalytic effect by a single metal ion. Supported by either an additional charge on the histidine residue or a metal ion on the attack site, however, direct nucleophilic attack, concerted with a proton transfer from the attacking water molecule to the phosphate group, shows reduced barriers compared to the uncatalyzed reaction. In contrast, leaving group departure is not facilitated by the presence of an extra positive charge. This can be explained by the protonation of the departing leaving group being preferable via proton transfer from the phosphate group. In contrast to proton transfer from metal-bound water molecules this step is not affected by the presence of a second metal ion.

The most favorable mechanism in either, one-metal or two-metal models, is via the attack of a hydroxide ion, generated by a histidine-assisted proton transfer. This proton transfer in turn, is enabled by the presence of an additional aspartate residue in hydrogen-bonding, and hence proton-accepting distance to the histidine residue. Attack of the hydroxide ion without proton transfer to the phosphate group is then facilitated by the metal ions. In the case of the single metal located at the departure site, nucleophilic attack and leaving group departure take place in one step. A pentacovalent intermediate can be located only for the models with a metal ion located at the attack site, 1MgA or the two-metal model, rendering the presence of a metal ion at this location necessary for intermediate stabilization. Further catalysis of leaving group departure by a second metal ion results in the significantly lower barriers computed for the two-metal model compared to the one-metal case.

The composition of the catalytically most effective cluster model, 2Mg-Hsd-Glu-2Asp-1Asp, is comparable to known enzymatic architectures and the barrier computed for the energetically most favorable mechanism 2Mg-h is in agreement with rates reported for enzymatic phosphodiester cleavage.

The structural requirements for the energetically most feasible mechanism computed here illustrate the delicate orchestration necessary for optimal enzymatic function.

Acknowledgement

We gratefully acknowledge funding by the Deutsche Forschungsgemeinschaft (DFG) through grant IM141/1-1.

References

[1] Tatsuya Nishino and Kosuke Morikawa. Structure and function of nucleases in DNA repair: shape, grip and blade of the DNA scissors. *Oncogene.*, 21(58):9022–9032, 16 December 2002.

[2] B. Demple and L. Harrison. Repair of oxidative damage to DNA: Enzymology and biology. *Annu. Rev. Biochem.*, 63:915–948, July 1994.

[3] D.J. Hosfield, Y. Guan, B.J. Haas, R.P. Cunningham, and J.A. Tainer. Structure of the DNA repair enzyme endonuclease IV and its DNA complex: Double-nucleotide flipping at abasic sites and three-metal-ion catalysis. *Cell.*, 98(3):397–408, August 1999.

[4] L. Nilsen, R.J. Forstrom, M. Bjoras, and I. Alseth. AP endonuclease independent repair of abasic sites in schizosaccharomyces pombe. *Nucleic Acids Res.*, 40(5):2000–2009, March 2012.

[5] H. Korhonen, S. Mikkola, and N. H. Williams. The mechanism of cleavage and isomerization of RNA promoted by an efficient dinuclear zn^{2+} complex. *Chem Eur J.*, 18:659–670, 2012.

[6] Barbara L. Golden. Two distinct catalytic strategies in the hepatitis delta virus ribozyme cleavage reaction. *Biochemistry*, 50(44):9424–9433, 2011.

[7] Jesse C. Cochrane and Scott A. Strobel. Catalytic strategies of self-cleaving ribozymes. *Acc. Chem. Res.*, 41(8):1027–1035, 2008.

[8] Jan Florián, Johan Åqvist, and Arieh Warshel. On the reactivity of phosphate monoester dianions in aqueous solution: Bronsted linear free-energy relationships do not have an unique mechanistic interpretation. *J. Am. Chem. Soc.*, 120:11524–11525, 1998.

[9] Jan Florián, Marek Strajbl, and Arieh Warshel. Conformational flexibility of phosphate, phosphonate, and phosphorothioate methyl esters in aqueous solution. *J. Am. Chem. Soc*, 120:7959–7966, 1998.

[10] Jan Florián and Arieh Warshel. Phosphate ester hydrolysis in aqueous solution: associative versus dissociative mechanisms. *J. Phys. Chem. B.*, 102:719–734, 1998.

[11] Piotr Grzyska, Przemyslaw G. Czyryca, Jamie Purcell, and Alvan C. Hengge. Transition state differences in the hydrolysis reactions of alkyl versus aryl phosphate monoester monoanions. *J. Am. Chem. Soc*, 125:13106–13111, 2003.

[12] Ching-Han Hu and Tore Brinck. Theoretical studies of the hydrolysis of the methyl phosphate anion. *J. Phys. Chem. A.*, 103:5379–5386, 1999.

[13] Tim Humphry, Marcello Forconi, Nicholas H. Williams, and Alvan C. Hengge. An altered mechanism of hydrolysis for a metal-complexed phosphate diester. *J. Am. Chem. Soc*, 124:14860–14861, 2002.

[14] Petra Imhof, Stefan Fischer, Roland Krämer, and Jeremy C. Smith. Density functional theory analysis of dimethylphosphate hydrolysis: effect of solvation and nucleophile variation. *J. Mol. Struct. (Theochem.)*, 713:1–5, 2004.

[15] Jose M. Mercero, Paul Barrett, Cheuk W. Lam, Joseph E. Fowler, Jesus M. Ugalde, and Lee G. Pedersen. Quantum mechanical calculations on phosphate hydrolysis reactions. *J. Comput. Chem.*, 21:43–51, 2000.

[16] Nathalie Iche-Tarrat, Jean-Claude Barthelat, Daniel Rinaldi, and Alain Vigroux. Theoretical studies of the hydroxide-catalyzed P-O cleavage reactions of neutral phosphate triesters and diesters in aqueous solution: Examination of the changes induced by H/Me substitution. *J. Phys. Chem. B.*, 109:22570–22580, 2005.

[17] Patrick J. O'Brien and Daniel Herschlag. Alkaline phosphatase revisited: Hydrolysis of alkyl phosphates. *Biochem.*, 41:3207–3225, 2001.

[18] James Borden, Debbie C. Crans, and Jan Florian. Transition state analogues for nucleotidyl transfer reactions: Structure and stability of pentavalent vanadate and phosphate ester dianions. *J. Phys. Chem. B*, 110(30):14988–14999, 2005.

[19] A. Peck, F. Sunden, L.D. Andrews, V.S. Pande, and D. Herschlag. Tungstate as a transition state analog for catalysis by alkaline phosphatase. *J. Mol. Biol*, 428:2758–2768, 2016.

[20] Emmanuel Y. Tirel and Nicholas H. Williams. Enhancing phosphate diester cleavage by a zinc complex through controlling nucleophile coordination. *Chemistry - A European Journal*, 21(19):7053–7056, 2015.

[21] Letif Mones, Petr Kulhanek, Jan Florian, Istvan Simon, and Monika Fuxreiter. Transition state analogues for nucleotidyl transfer reactions: Structure and stability of pentavalent vanadate and phosphate ester dianions. *Biochemistry*, 46(50):14514–14523, 2007.

[22] Jonathan K. Lassila, Jesse G. Zalatan, and Daniel Herschlag. Biological phosphoryl-transfer reactions: Understanding mechanism and catalysis. *Ann. Rev. Biochem.*, 80:669, 2011.

[23] Roland K. O. Sige and Anna Marie Pyle. Alternative roles for metal ions in enzyme catalysis and the implications for ribozyme chemistry. *Chem. Rev*, 107(1):97–113, 2007.

[24] Mauro Boero, Masaru Tateno, Kiyoyuki Terakura, and Atsushi Oshiyama. Double-metal-ion/single-metal-ion mechanisms of the cleavage reaction of ribozymes: First-principles molecular dynamics simulations of a fully hydrated model system. *Journal of Chemical Theory and Computation*, 1(5):925–934, 2005.

[25] Giulia Palermo amd Andrea Cavalli, Michael L. Klein, Mercedes Alfonso-Prieto, Matteo Dal Peraro, and Marco De Vivo. Catalytic metal ions and enzymatic processing of dna and rna. *Accounts of Chemical Research*, 48(2):220–228, 2015.

[26] Shiyan Xiao, Michael L. Klein, David N. LeBard, Benjamin G. Levine, Haojun Liang, Christopher M. MacDermaid, and Mercedes Alfonso-Prieto. Magnesium-dependent rna binding to the pa endonuclease domain of the avian influenza polymerase. *The Journal of Physical Chemistry B*, 118(4):873–889, 2014.

[27] Lorenzo Casalino, Giulia Palermo, Ursula Rothlisberger, and Alessandra Magistrato. Who activates the nucleophile in ribozyme catalysis? an answer from the splicing mechanism of group ii introns. *Journal of the American Chemical Society*, 138(33):10374–10377, 2016.

[28] Anna Lopata, Pablo G. Jambrina, Pankaz K. Sharma, Bernard R. Brooks, Judit Toth, Beata G. Vertessy, and Edina Rosta. Mutations decouple proton transfer from phosphate cleavage in the dutpase catalytic reaction. *ACS Catalysis*, 5(6):3225–3237, 2015.

[29] Fan Zhang, Nanhao Chen, Jingwei Zhou, and Ruibo Wu. Protonation-dependent diphosphate cleavage in fpp cyclases and synthases. *ACS Catalysis*, 6(10):6918–6929, 2016.

[30] Anthony J. Kirby and Faruk Nome. Fundamentals of phosphate transfer. *Acc. Chem. Res.*, 48(7):1806–1814, 2015.

[31] Hongzhen He, Qiujia Chen, and Millie M. Georgiadis. High-resolution crystal structures reveal plasticity in the metal binding site of apurinic/apyrimidinic endonuclease I. *Biochem.*, 53:6520–6529, September 2014.

[32] P. T. Beernink, B. W. Segelke, M. Z. Hadi, J. P. Erzberger, D. M. Wilson, and B. Rupp. Two divalent metal ions in the active site of a new crystal form of human apurinic/apyrimidinic endonuclease, Ape1: implications for the catalytic mechanism. *J. Mol. Biol.*, 307(4):1023–1034, July 2001.

[33] Gil Barzilay and Ian D. Hickson. Structure and function of apurinic/apyrimidinic endonucleases. *BioEssays.*, 17:713–719, 1995.

[34] E.D. Garcin, D. J. Hosfield, S. A. Desai, B. J. Haas, M. Bjoras, R. P. Cunningham, and J. A. Tainer. Dna apurinic-apyrimidinic site binding and excision by endonuclease IV. *Nat. Struct. Mol. Biol.*, 15:515–522, April 2008.

[35] Bret D. Freudenthal, William A. Beard, Matthew J. Cuneo, Nadezhda S. Dyrkheeva, and Samuel H. Wilson. Capturing snapshots of APE1 processing DNA damage. *Nature Struct. Mol. Biol.*, 22:924–931, 2015.

[36] J.M. Hadden, A. C. Declais, S. E. Phillips, and D. M. Lilley. Metal ions bound at the active site of the junction-resolving enzyme T7 endonuclease I. *EMBO J.*, 21:3505–3515, 2002.

[37] S.E. Tsutakawa, H. Jingami, and K. Morikawa. Recognition of a TG mismatch: the crystal structure of very short patch repair endonuclease in complex with a DNA duplex. *Cell.*, 99(6):615–623, December 1999.

[38] W.P. Jencks. *Catalysis in Chemistry and Enzymology.* McGraw Hill., New York, 1969.

[39] K. Katayanagi, M. Okumura, and K. Morikawa. Crystal structure of escherichia coli RNase HI in complex with Mg^{2+} at 2.8 å resolution: proof for a single Mg^{2+}-binding site. *Proteins.*, 17(4):337–46, December 1993.

[40] Mai Zahran, Tomasz Berezniak, Petra Imhof, and Jeremy C. Smith. Role of magnesium ions in DNA recognition by the EcoRV restriction endonuclease. *FEBS Lett.*, 585(17):2739–2743, September 2011.

[41] R.A. Kovall and B.W. Matthews. Type II restriction endonucleases: structural, functional and evolutionary relationships. *Curr. Opin. Chem. Biol.*, 3(5):578–583, October 1999.

[42] Sinead M. Kerins, Ruairi Collins, and Tommie V. McCarthy. Characterization of an endonuclease IV. *J. Biol. Chem.*, 278:3048–3054, 2003.

[43] Mary R Stahley and Scott A Strobel. RNA splicing: group I intron crystal structures reveal the basis of splice site selection and metal ion catalysis. *Curr. Opin. Struct. Biol.*, 16(3):319–326, 2006.

[44] Jae Young Lee, Judy Chang, Nimesh Joseph, Rodolfo Ghirlando, Desirazu N. Rao, and Wei Yang. Muth complexed with hemi- and unmethylated DNAs: Coupling base recognition and DNA cleavage. *Mol. Cell.*, 20:155–166, October 2005.

[45] L S Beese and T A Steitz. Structural basis for the 3-'-5' exonuclease activity of escherichia coli DNA polymerase I: a two metal ion mechanism. *EMBO J.*, 10(1):25–33, 1991.

[46] M. Nowotny and W. Yang. Stepwise analyses of metal ions in RNase H catalysis from substrate destabilization to product release. *EMBO J.*, 25(9):1924–1933, 2006.

[47] Anastasia D. Miroshnikova, Alexandra A. Kuznetsova, Yuri N. Vorobjev, Nikita A. Kuznetsov, and Olga S. Fedorova. Effects of mono- and divalent metal ions on DNA binding and catalysis of human apurinic/apyrimidinic endonuclease 1. *Mol. BioSyst.*, 12:1527–1539, 2016.

[48] Numan Oezguen, Catherine H. Schein, Srinivasa R. Peddi, Trevor D. Power, Tadahide Izumi, and Werner Braun. A "moving metal mechanism" for substrate cleavage by the DNA repair endonuclease APE-1. *Proteins: Structure, Function, and Bioinformatics*, 68(1):313–323, 2007.

[49] Numan Oezguen, Anil K. Mantha, Tadahide Izumi, Catherine H. Schein, Sankar Mitra, and Werner Braun. MD simulation and experimental evidence for Mg^{2+} binding at the b site in human AP endonuclease 1. *Bioinformation*, 7(4):184–198, 2011.

[50] Eric A. Galburt, Brett Chevalier, Weiliang Tang, Melissa S. Jurica, Karen E. Flick, Jr. Raymond J. Monnat, and Barry L. Stoddard. A novel endonuclease mechanism directly visualized for I-PpoI. *Nat. Struct. Biol.*, 6(12):1096–1999, 1999.

[51] M.D. Miller, J. Tanner, M. Alpaugh M.J. Benedik, and K.L. Krause. 2.1 å structure of serratia endonuclease suggests a mechanism for binding to double-stranded DNA. *Nat. Struct. Mol. Biol.*, 1:461–468, 1994.

[52] Jennifer H. Eastberg, Jennifer Eklund, Jr Raymond Monnat, and Barry L. Stoddard. Mutability of an HNH nuclease imidazole general base and exchange of a deprotonation mechanism. *Biochemistry*, 46(24):7215–7225, 2007.

[53] B. R. Brooks, III C. L. Brooks, A. D. Mackerell, L. Nilsson, R. J. Petrella, B. Roux, Y. Won, G. Archontis, C. Bartels, S. Boresch, A. Caflisch, L. Caves, Q. Cui, A. R. Dinner, M. Feig, S. Fischer, J. Gao, M. Hodoscek, W. Im, K. Kuczera, T. Lazaridis, J. Ma, V. Ovchinnikov, E. Paci, R. W. Pastor, C. B. Post, J. Z. Pu, M. Schaefer, B. Tidor, R. M. Venable, H. L. Woodcock, X. Wu, W. Yang, D. M. York, and M. Karplus. The biomolecular simulation program. *J. Comput. Chem.*, 30:1545–1615, 2009.

[54] Qiang Cui, Marcus Elstner, Efthimios Kaxiras, Thomas Frauenheim, and Martin Karplus. A qm/mm implementation of the self-consistent charge density functional tight binding (SCC-DFTB) method. *J. Phys. Chem. B.*, 105(2):569–585, 2001.

[55] Michael Gaus, Xiya Lu, Marcus Elstner, and Qiang Cui. Parameterization of DFTB3/3OB for sulfur and phosphorus for chemical and biological applications. *J. Chem. Theory Comput.*, 10(4):1518–1537, 2014.

[56] Stefan Fischer and Martin Karplus. Conjugate peak refinement: an algorithm for finding reaction paths and accurate transition states in systems with many degrees of freedom. *Chem. Phys. Lett.*, 194:252–261, 1992.

[57] Chengteh Lee, Weitao Yang, and Robert G. Parr. Development of the colle-salvetti correlation-energy formula into a functional of the electron density. *Phys. Rev. B.*, 37:785, 1988.

[58] Axel D. Becke. Density-functional thermochemistry. III. the role of exact exchange. *J. Chem. Phys.*, 98:5648, 1993.

[59] P.C. Hariharan and J.A. Pople. The influence of polarization functions on molecular orbital hydrogenation energies. *Theor. Chem. Acc.*, 28(3):213–222, September 1973.

[60] M. J. Frisch, G. W. Trucks, H. B. Schlegel, G. E. Scuseria, M. A. Robb, J. R. Cheeseman, G. Scalmani, V. Barone, B. Mennucci, G. A. Petersson, H. Nakatsuji, M. Caricato, X. Li, H. P. Hratchian, A. F. Izmaylov, J. Bloino, G. Zheng, J. L. Sonnenberg, M. Hada, M. Ehara, K. Toyota, R. Fukuda, J. Hasegawa, M. Ishida, T. Nakajima, Y. Honda, O. Kitao, H. Nakai, T. Vreven, J. A. Montgomery Jr., J. E. Peralta, F. Ogliaro, M. Bearpark, J. J. Heyd, E. Brothers, K. N. Kudin, V. N. Staroverov, R. Kobayashi, J. Normand, K. Raghavachari, A. Rendell, J. C. Burant, S. S. Iyengar, J. Tomasi, M. Cossi, N. Rega, J. M. Millam, M. Klene, J. E. Knox, J. B. Cross, V. Bakken, C. Adamo, J. Jaramillo, R. Gomperts, R. E. Stratmann, O. Yazyev, A. J. Austin, R. Cammi, C. Pomelli, J. W. Ochterski, R. L. Martin, K. Morokuma, V. G. Zakrzewski, G. A. Voth, P. Salvador, J. J. Dannenberg, S. Dapprich, A. D. Daniels, O. Farkas, J. B. Foresman, J. V. Ortiz, J. Cioslowski, and D. J. Fox. Gaussian, inc., wallingford ct, 2009.

[61] E.D. Glendening, A.E. Read, J.E. Carpenter, and F. Weinhold. Nbo (version 3.1), 2009.

[62] Petra Imhof, Stefan Fischer, Roland Krämer, and Jeremy C. Smith. Density functional theory analysis of dimethylphosphate hydrolysis: effect of solvation and nucleophile variation. *J. Mol. Struct. (Theochem.)*, 713:1–5, January 2005.

[63] Petra Imhof, Stefan Fischer, and Jeremy C. Smith. Catalytic mechanism of DNA backbone cleavage by the restriction enzyme EcoRV: A quantum mechanical/molecular mechanical analysis. *Biochem.*, 48(38):9061–9075, September 2009.

[64] David F. Lowry, David W. Hoyt, Fayaz A. Khazi, John Bagu, Andrea G. Lindsey, and David M. Wilson III. Investigation of the role of the histidine-aspartate pair in the human exonuclease III-like abasic endonuclease Ape1. *J. Mol. Biol*, 329(2):311–322, May 2003.

[65] Marie-Josephe E. Giraud-Panis and David M. J. Lilley. T4 endonuclease VII importance of a histidine-aspartate cluster within the zinc-binding domain. *J. Biol. Chem.*, 271:33148–33155, December 1996.

[66] Shina C. L. Kamerlin, Nicholas H. Williams, and Arieh Warshel. Dineopentyl phosphate hydrolysis: Evidence for stepwise water attack. *J. Org. Chem*, 73(18):6960–6969, 2008.

[67] M. Klahn, E. Rosta, and A. Warshel. On the mechanism of hydrolysis of phosphate monoester dianions in solution and proteins. *J. Am. Chem. Soc*, 128:15310–15323, 2006.

[68] Fernanda Duarte, Johan Aqvist, Nicholas H. Williams, and Shina C. L. Kamerlin. Resolving apparent conflicts between theoretical and experimental models of phosphate monoester hydrolysis. *J. Am. Chem. Soc*, 137(3):1081–1093, 2015.

[69] Anthony J. Kirby, Michelle Medeiros, Jose R. Mora, Pedro S. M. Oliveira, Almahdi Amer, Nicholas H. Williams, and Faruk Nome. Intramolecular general base catalysis in the hydrolysis of a phosphate diester. calculational guidance to a choice of mechanism. *J. Org. Chem*, 78(4):1343–1353, 2013.

[70] Jacopo Sgrignani and Alessandra Magistrato. Qm/mm md simulations on the enzymatic pathway of the human flap endonuclease (hfen1) elucidating common cleavage pathways to rnase h enzymes. *ACS Catalysis*, 5(6):3864–3875, 2015.

[71] M. Takeuchi, R. Lillis, B. Demple, and M. Takeshita. Mammalian abasic site base excision repair. *J. Biol. Chem.*, 269(34):21907–21914, August 1998.

[72] IVIvaylo Ivanov, John A. Tainer, and J. Andrew McCammon. Unraveling the three-metal-ion catalytic mechanism of the DNA repair enzyme endonuclease IV. *PNAS.*, 104(5):1465–1470, 2007.

[73] C.D. Mol, T. Izumi, S. Mitra, and J.A. Tainer. DNA-bound structures and mutants reveal abasic DNA binding by APE1 DNA repair and coordination. *Nature.*, 403:451–456, January 2000.

[74] Jesse G. Zalatan and Daniel Herschlag. Alkaline phosphatase mono- and diesterase reactions: Comparative transition state analysis. *J. Am. Chem. Soc*, 128(4):1293, 2006.

[75] Guanhua Hou and Qiang Cui. QM/MM analysis suggests that alkaline phosphatase (AP) and nucleotide pyrophosphatase/phosphodiesterase slightly tighten the transition state for phosphate diester hydrolysis relative to solution: Implication for catalytic promiscuity in the AP superfamily. *J. Am. Chem. Soc*, 134(1):229–246, 2012.

[76] Adam G. Cassano, Vernon E. Anderson, and Michael E. Harris. Evidence for direct attack by hydroxide in phosphodiester hydrolysis. *J. Am. Chem. Soc.*, 124(37):10964–10965, 2002.

[77] Y. Cheng and D. J. Patel. Crystallographic structure of the nuclease domain of 3'hExo, a DEDDh family member, bound to rAMP. *J. Mol. Biol*, 343(2):305–312, 2004.

[78] M. Dlakic. Functionally unrelated signalling proteins contain a fold similar to Mg^{2+}dependent endonucleases. *Trends Biochem. Sci.*, 25(272-273):272–273, 2000.

[79] C.D. Mol, C.F. Kuo, M.M. Thayer, R.P. Cunningham, and J.A. Tainer. Structure and function of the multifunctional DNA-repair enzyme exonuclease III. *Nature.*, 374:381–386, 1995.

[80] Chia-Lung Li, Lien-I Hor, Zee-Fen Chang, Li-Chu Tsai, Wei-Zen Yang, and Hanna S. Yuan. DNA binding and cleavage by the periplasmic nuclease Vvn: a novel structure with a known active site. *EMBO J.*, 22(15):4014–4025, 2003.